Front. Optoelectron. 2012, 5(2): 127–132
DOI 10.1007/s12200-012-0256-z

RESEARCH ARTICLE

High-performance and current crowding-free InGaN-GaN-based LEDs integrated by an electrically-reverse-connected Schottky diode and a Mg-delta doped *p*-GaN

Sei-Min KIM, Seon-Ho JANG, Ja-Soon JANG (✉)

Department of Electronic Engineering, LED-IT Fusion Technology Research Center (LIFTRC), Yeungnam University, Gyeongbuk 712–749, Korea

© Higher Education Press and Springer-Verlag Berlin Heidelberg 2012

Abstract This work demonstrates high-performance and current crowding-free InGaN/GaN light-emitting diodes (LEDs) using an electrically-reverse-connected Schottky diode (SD) and an Mg-delta (δ) doped layer. Possible mechanism of carrier transport at the interface between transparent conducting electrode (TCE) and *p*-GaN with the δ-doped layer is also investigated. Results show that the LED with the SD and Mg delta (δ)-doping layer yields lower series resistance, higher output power, and lower reverse leakage current compared to normal LEDs. In addition, unlike the normal LED, there is no occurrence for the current crowding effect in the proposed LED even at high current density of 380 mA/cm^2. These remarkable behaviours clearly indicate that the use of the SD and δ-doping in the *p*-GaN region is very promising to achieve high-brightness and excellent-reliability GaN-based LEDs.

Keywords GaN, light-emitting diode (LED), Schottky diode (SD), integration, current crowding

1 Introduction

High-performance GaN-based light emitting diodes (LEDs) with high efficiency and excellent reliability have been of technological importance for applications in full color display, automotive lighting, and solid state lighting [1]. In particular, due to fundamental drawbacks such as low Mg-activated carrier concentration (by low activation efficiency of Mg-H complex) and low *p*-ohmic contact resistance [2–4], GaN-based LEDs having a lateral current path suffer from the current crowding, high turn-on voltage, and high leakage current. To resolve these problems, InGaN-GaN and AlGaN-GaN superlattices (SLs) incorporated into GaN-based LED structures [5–9] have been extensively investigated. It was found that Mg-doped (Al, In)GaN-GaN SLs lead to a considerable improvement in the overall device properties such as output power and turn-on voltage by an improvement of high conductivity of these SLs, originating from an increased acceptor concentration by polarization effect in the strain-induced layers on *p*-GaN [7].

Recently, according to Jang [10], the use of the electrically reverse-connected Schottky diode (SD) as well as the SLs is very effective to reduce defect-related influence and hence improve the device reliability characteristics of GaN-based LEDs if the SD on *p*-GaN is electrically reverse-operated. In fact, the GaN-based LEDs suffer from various defects such as threading dislocations and various point defects [4,11–13]. These defects could affect forward/reverse leakage current and device reliability characteristics during the device operation. Thus, to develop high-efficiency and high-reliability GaN-based LEDs, how to reduce defect-related influence as well as how to improve *p*-conductivity should be taken into account.

Mg delta (δ)-doping in *p*-GaN has been considerably attractive because of the fact that the δ-doping is very effective in obtaining high hole concentration ($\geqslant 1 \times 10^{18}$ cm^{-3}) of *p*-GaN [14–17]. In other words, the δ-doping can be a good candidate for replacing the SLs in *p*-GaN regions of GaN-based LEDs. The improvement of the hole concentration is due to the reduction in the Mg activation energy and self-compensation effects in δ-doped GaN [16]. Therefore, in this paper, we have investigated the SD and δ-doping influence on the electrical and optical characteristics of GaN-based LEDs. Possible carrier transport mechanism at the interface between transparent conducting electrode (TCE) and *p*-GaN containing the *d*-doped layer is also discussed using specific contact resistance-temperature (R_{sc}-T) and current-voltage-temperature (I-V-T) data. It

Received November 28, 2011; accepted December 8, 2011

E-mail: jsjang@ynu.ac.kr

is found that the integration of the SD and the Mg δ-doping in the *p*-GaN layer produce the high device performance characteristics including that there is no occurrence in the current crowding even at high current density of 380 mA/cm^2.

2 Operational mechanism for SD-integrated GaN-based LEDs with Mg δ-doped GaN layer

Figure 1 shows schematic cross-sectional diagram, electrically equivalent circuit, and possible current path of the normal LED and the SD-integrated LED having the δ-doped layer. For simplicity, a LED without/with the SD and δ-doped layer is named here as a normal LED and a δ-SD LED, respectively. As for the normal LED (Fig. 1(a)), Ni/Au bonding pad is directly formed on indium tin oxide/nickel oxide (ITO/NiO_x) TCE. On the contrary, for the δ-SD LED as shown in Fig. 1(b), the Schottky electrode on *p*-GaN (like n^+-p diode) is electrically reversed to the GaN-based LED. Unlike the normal LED operation (Fig. 1(c)), if a reverse differential resistance ($\mathrm{d}V/\mathrm{d}I$) of the SD is high enough to act as a high-resistance resistor, it could be expected that most of the current is injected into the δ-SD LED through the ITO/δ-doped *p*-GaN TCE window during the forward LED operation (Fig. 1(d)). In addition, the use of the δ-doped layer in the LED could lead to an improvement of conductivity of *p*-contact layer and *p*-ohmic contact as described previously [14–17], thus, for this δ-SD LED structure, current injection density becomes larger, and hence current injection efficiency becomes better, as compared to the normal LED. Furthermore, an influence of parasitic defects existing in the *p*-current injected area of the LED could be effectively reduced by means of a current blocking-area of the SD, resulting in a decrease of leakage current and considerably improving the overall reliability characteristics of the LED.

3 Experiments

3.1 Fabrication of C-TLM patterns and measurements

In order to investigate the carrier transport mechanism at the interface between metals and GaN, circular-transmission line model (C-TLM) patterns were fabricated. Metal-organic chemical vapor deposition system was used to grow a 2 μm thick unintentionally (*u*)-doped GaN layer on a 30 nm thick GaN nucleation layer/(0001) sapphire substrate. For Mg-doped GaN, the 100 nm thick *p*-GaN layer was grown on the *u*-doped GaN. As for Mg δ-doped GaN, the 0.5 μm thick layers consisting of 35 periods was grown on the *u*-doped GaN layer. All samples were then rapid-thermal-annealed at 650°C for 10 min under nitrogen ambient to activate Mg dopants. Prior to the fabrication of C-TLM patterns, the surfaces of the all samples were ultrasonically degreased with acetone, methanol, and ethanol for 5 min in each step, and then rinsed with deionized water followed by N_2 blowing. Buffered oxide etch (BOE) surface treatment was ultrasonically carried out for 5 min at room temperature. C-TLM patterns were defined using a photolithographic technique. The inner radius of the C-TLM pad was 100 μm and the spacing between the inner and outer pads was 10, 15, 20, and 30 μm. Prior to the deposition of metal films, the C-TLM patterned layers were dipped into a BOE solution for 30 s. The Ni/Au (5/5 nm) metals were then deposited by an electron-beam evaporation and rapid-thermally annealed at 550°C to form NiO/*p*-GaN. After the formation of the NiO, the ITO (220 nm) film was deposited on the NiO by an electron-beam evaporation. *I-V* and *I-V-T* characteristics were measured using an on-wafer probing system having a hot chuck and a semiconductor analyzer (HP4155A).

3.2 Fabrication of LEDs and Measurements

Metal organic chemical vapour deposition (MOCVD) system was used to grow InGaN-GaN multiple quantum wells (MQWs) LED wafers with a peak wavelength of around 450 nm on c-face sapphire substrates. The LED epitaxial layers consist of a 30 nm thick GaN nucleation layer on sapphire substrate, a 2 μm thick unintentionally doped GaN layer, a 1.5 μm thick Si-doped GaN *n*-contact layer (N_d about 4×10^{18} cm^{-3}), an active region with five periods of InGaN-GaN MQWs, a 0.1-μm-thick Mg-doped GaN layer, and the 0.5-μm-thick Mg-δ doped *p*-contact layer consisting of 35 periods. The activated Mg concentration was determined to be 3.2×10^{17} and 0.93×10^{17} cm^{-3} for *p*-GaN and δ-doped *p*-GaN by means of Hall effect measurement. The LEDs (900 μm × 900 μm) were fabricated using photolithography patterning and inductive coupled plasma (ICP) etching to a depth of 1.1 μm. Unlike the normal LED, the second ICP etching (with a depth of 22 nm) was carried out to expose the *p*-GaN surface in the δ-SD LED. For normal LEDs, sputtered ITO films (220 nm)/electron-beam-evaporated Ni/Au (5/5 nm) layers were deposited on *p*-GaN as a transparent ohmic electrode and then were annealed at 550°C for 30 s in a N_2 ambience. Electron-beam-evaporated Ni/Au (30/300 nm) bonding-pad electrodes were deposited on the ITO/NiO ohmic electrode. However, for the δ-SD LED, the sputtered ITO layer on the δ-doped *p*-GaN were annealed at 550°C for 30 s in a N_2 ambience, and the electron-beam-evaporated Al (300 nm) scheme was formed on *p*-GaN as a *p*-SD. Cr/Ni/Au (20/30/300 nm) films as an *n*-ohmic electrode were deposited on n^+-GaN layer for all the LEDs. All the *p*- and *n*-electrodes were annealed at 500°C for 30 s in a flowing N_2 ambient. *I-V* data were obtained using a semiconductor parameter analyzer (HP4155A). Optical power-current (*L-I*) data were obtained using an optical spectrometer and a photodiode detector.

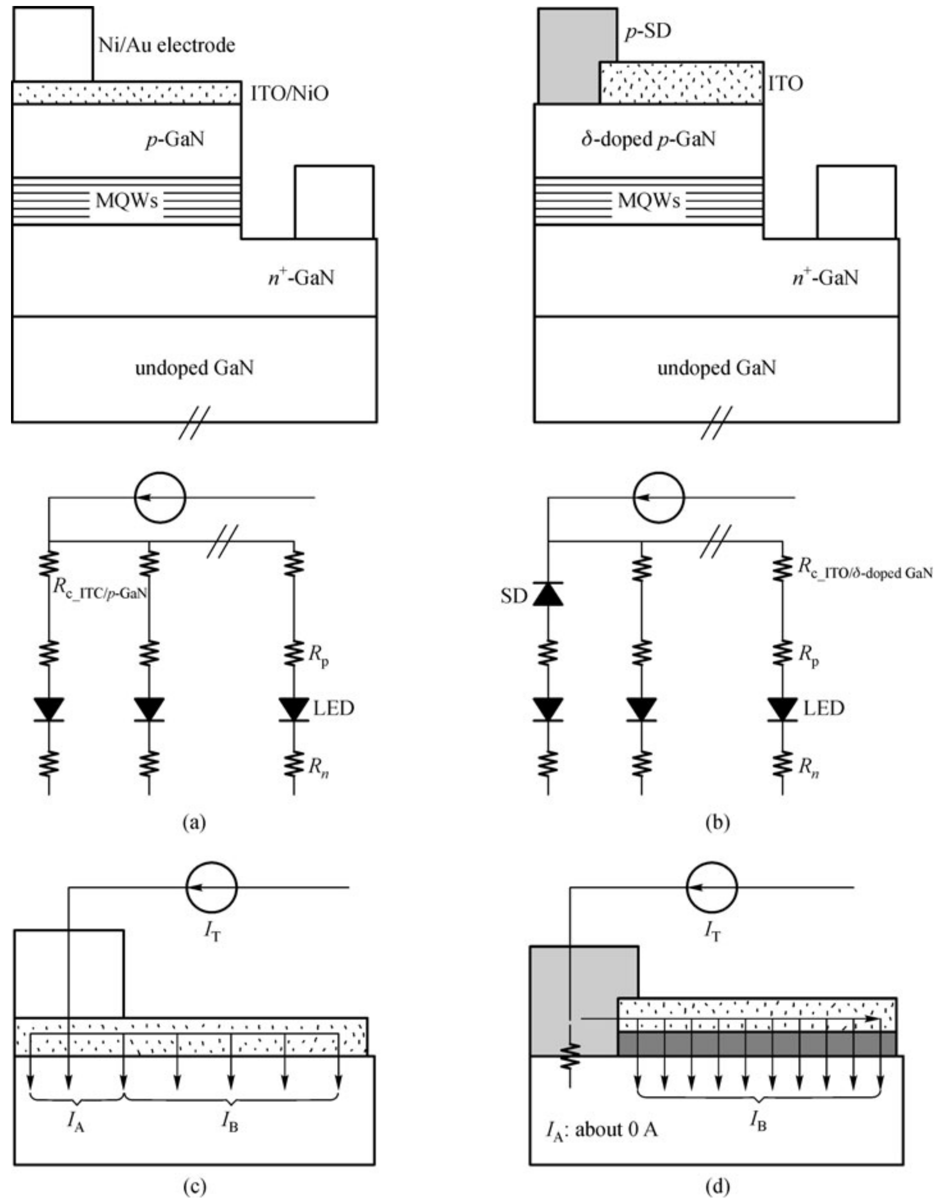

Fig. 1 (a) and (b) schematic cross-sectional diagram and electrically equivalent circuit of normal LED and δ-SD LED; (c) possible current injection path ($I_T = I_A + I_B$) of normal LED; and (d) that ($I_T \approx I_B$) of δ-SD LED if the resistance of *p*- SD is assumed to be much higher, during the forward operation

4 Carrier transport mechanism at the interface between TCE and δ-doped *p*-GaN

Figure 2 shows the *I-V* characteristics for the *p*-GaN and the δ-doped GaN contacts. The *p*-GaN contact exhibits a nonlinear *I-V* behavior, while the δ-doped *p*-GaN contact displays a linear *I-V* characteristic. The specific contact resistance (R_{sc}) was determined from a plot of the measured resistances vs. the spacing between C-TLM patterns. The C-TLM method was used to fit a log-scaled line to the experimental data [18]. The R_{sc} was obtained to be 1.5×10^{-2} and $2.3\times10^{-5}\ \Omega\cdot\text{cm}^2$ for the *p*-GaN and δ-doped *p*-GaN contacts, respectively. It should be stressed that the use of the δ-doping yields a dramatic improvement of the R_{sc}, revealing that it is very promising to achieve high-quality ohmic electrodes. Unlike the *p*-GaN contact, the improvement in the *I-V* curves for the δ-doped *p*-GaN contact can be closely associated with a high-accumulated acceptor concentration in the δ-doped GaN surface [16]. Thus, high hole concentrations (about $10^{18}\ \text{cm}^{-3}$) increase a hole-tunneling probability at the interface between ITO/NiO and δ-doped *p*-GaN, and hence result in the linear *I-V*

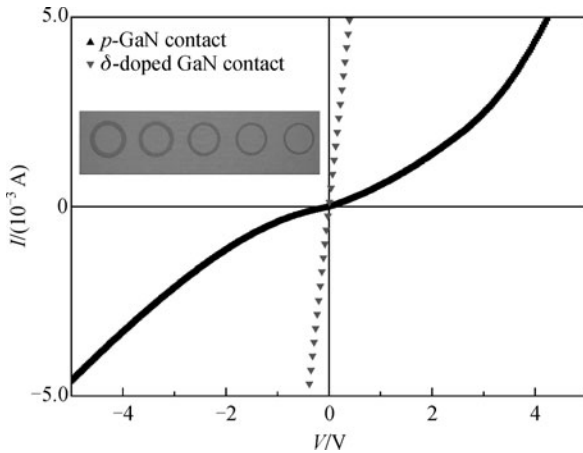

Fig. 2 Current-voltage (*I-V*) characteristics for *p*-GaN and *δ*-doped GaN contacts; and the inset shows a photograph of C-TLM patterns

behavior.

To interpret the carrier transport mechanism for the *p*-GaN and *δ*-doped GaN contacts in detail, a metal/p^+-/*p*-GaN model was employed [19]. In this model, the high-accumulated hole region in the *δ*-doped *p*-GaN is assumed to have p^+-GaN. A carrier distribution function of the p^+-region is also assumed to be $N_{\mathrm{a}_p^+\text{-region}}(x) = N_0 \cdot \exp(-x/d)$. More detailed model information can be referred in Ref. [19]. In this work, we used two carrier transport models such as thermionic emission (TE) and field emission (FE) [19,20]. Figure 3 exhibits plots of the experimental and theoretical values of the R_{sc} as a function of $1/T$ using a metal/p^+-/*p*-GaN model. Comparisons show that the theoretical results are in good agreement with experimental data, indicating that our modeling is valid. The TE conduction is considerably dominant for the *p*-GaN contact, while the FE conduction is sensitively dominant for the *δ*-doped GaN contact. The results mean that the *δ*-doping in the *p*-GaN is very effective in increasing holes near the GaN surface as compared to the *p*-GaN contact. Larger hole-accumulation gives rise to the reduced barrier width and energy band-bending ($E_F - E_v$), and consequently results in tunneling of carriers at the interface. More detailed results will be published elsewhere [21].

5 Device characteristics for *p*-SD and *δ*-SD LED and discussion

Figure 4 shows the *I-V* characteristic of the Al (300 nm) Schottky contact on *p*-GaN as a *p*-SD. In this study, Pt/Ni/Au (20/30/100 nm) scheme was employed to form ohmic contact [22]. The rectifying *I-V* characteristic of the non-alloyed Al SD is indicative of the formation of Schottky contact at the interface between Al and GaN. A dynamic resistance of d*V*/d*I* for the forward-biased *I-V* curve was calculated to be more than 1 MΩ, indicating that the SD is good enough to act as a high-resistance resistor as described from Fig. 1.

Table 1 shows the summary of electrical data for both the normal and the *δ*-SD LED. It is shown that the mean turn-on voltage (V_{th}) of the normal LED is 4.0 V at 200 mA, while that of the *δ*-SD LED is 3.3 V. It is noted that the use of *p*-SD and *δ*-doping in the *p*-GaN produces a considerable reduction of the V_{th}. Series resistances of the LEDs were calculated using the relation, $I(\mathrm{d}V/\mathrm{d}I) = IR_s + nkT/q$, where R_s is series resistance and n is ideality factor. Calculations show that the mean R_s of the normal LEDs is 7.1 Ω, while that of *δ*-SD LED is 2.7 Ω. A considerable improvement of the R_s and V_{th} for the *δ*-SD LED (as

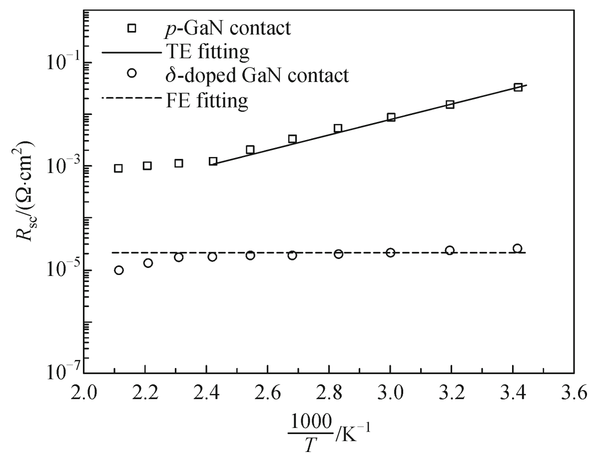

Fig. 3 Plots of experimental and theoretical values of R_{sc} as a function of $1/T$ using a metal/p^+-/*p*-GaN model. Dot line and solid line mean FE and TE fitting curves. TE is relatively dominant for *p*-GaN contact, while FE is considerably dominant for *δ*-doped GaN contact

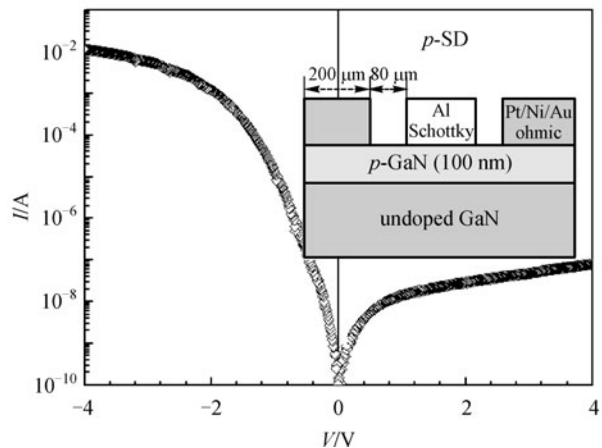

Fig. 4 Current-voltage (*I-V*) characteristics for Al/*p*-GaN SD, and the schematic cross-sectional diagram of the test pattern of the Schottky contact is shown in the inset

Table 1 Summary of electrical data obtained from normal and δ-SD LED

	V_{th}/V at 200 mA	R_s/Ω	n	I_F/nA at 2 V	I_R/nA at −5 V
normal LED	4.0±0.06	7.1±0.2	7.7±0.4	32±5	−42±6
δ-SD LED	3.3±0.07	2.7±0.3	2.5±0.5	3±2	−6±4

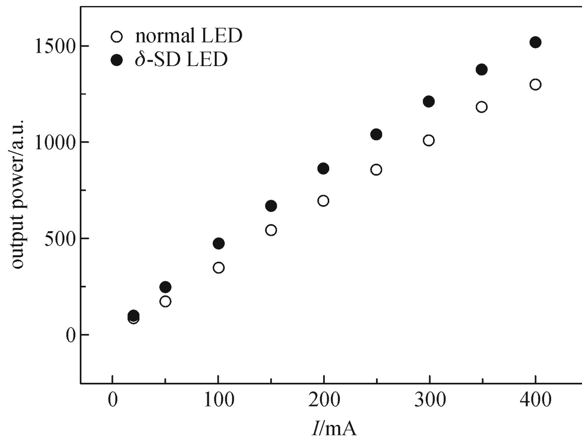

Fig. 5 Output power-current (L-I) characteristics of normal LED and δ-SD LED

compared to that of the normal LED) could be due to an improvement of p-conduction by an increased acceptor concentration and an increased current injection density (by using the high-resistance SD). As for the ideality factor, the mean n of the normal LED is calculated to be 7.7, whereas that of the δ-SD LED is 2.5. This implies that the SD is very effective to reduce the parasitic defect-related effect during the forward operation as illustrated from Fig. 1. In addition, these behaviours can also give appropriate explanations why the reverse leakage (at −5 V) and forward leakage (at 2 V) currents of the δ-SD LED are much lower than those of the normal LEDs in Table 1.

The output L-I characteristics of the LEDs are shown in Fig. 5. A comparison of the L-I data shows that the output power of the δ-SD LED (at 200 mA) is higher than that of both the normal LED by about 20%. In this work, light-transmittance (at 450 nm) of the ITO/NiO/p-GaN and ITO/δ-doped p-GaN was comparable and the value was around 91%. Based on I-V characteristics, L-I data, and light-transmittance results, it can be concluded that higher output power could be attributed to an increased current injection density as well as high-conduction δ-doped GaN.

Figure 6 shows the optical emission photographs obtained from the normal and the δ-SD LED. Unlike the normal LED suffering from severe current crowding effect, the δ-SD LEDs do not experience any current crowding effect even at high current density of 380 mA/cm^2. These behaviours indicate that the SD-integration and the Mg δ-doping in the p-GaN lead to very stable device-operation characteristics as compared to the normal LEDs without them. In this work, we also investigated the SD area dependence on the current crowding effect of the SD-integrated LEDs with/without δ-doped GaN layer. The results (not shown here) showed that the current crowding phenomena of the SD-integrated LEDs without a δ-doped GaN layer are sensitively affected by the ratio of the SD

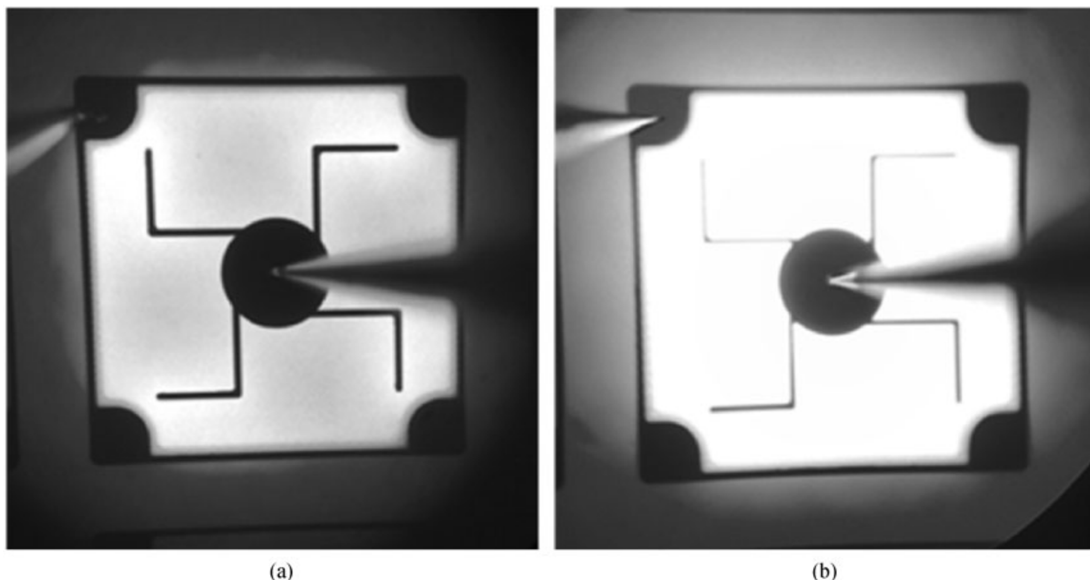

Fig. 6 Optical emission photographs obtained from (a) normal and (b) δ-SD LED at 380 mA/cm^2

and TCE window area. On the other hand, there is no occurrence for current crowding effect in the SD-integrated LEDs having the *d*-doped GaN layer irrespective of current density range up to 400 mA/cm^2. Thus, it can be concluded that the current crowding phenomena is absolutely affected by an electrically *p*-conduction in LEDs rather than others including the SD integration.

6 Conclusions

In summary, this paper successfully demonstrated the high-performance and current crowding-free InGaN/GaN LEDs using an electrically-reverse-connected SD and an Mg δ-doped GaN layer. Possible carrier transport mechanism at the interface between TCE and *p*-GaN with/without the δ-doped layer was also described. From the electrical and optical investigation results, the use of the SD and δ-doping in the *p*-GaN region is very practical to realize current crowding-free and high-efficiency GaN-based LEDs.

Acknowledgements This work was supported in part by the Ministry of Knowledge & Economy (MKE) through the industrial infrastructure program for fundamental technologies (No. 10033630) and through the part and material development program (No. 211C000553).

References

1. Nakamura S, Senoh S, Iwasa N, Nagahama S. High-brightness InGaN blue, green and yellow light-emitting diodes with quantum well structures. Japanese Journal of Applied Physics, 1995, 34(Part 2, No. 7A): L797–L799
2. Pearton S J, Zolper J C, Shul R J, Ren F. GaN: processing, defects, and devices. Journal of Applied Physics, 1999, 86(1): 1–78
3. Guo X, Schubert E F. Current crowding and optical saturation effects in GaInN/GaN light-emitting diodes grown on insulating substrates. Applied Physics Letters, 2001, 78(21): 3337
4. Wu J Q. When group-III nitrides go infrared: new properties and perspectives. Journal of Applied Physics, 2009, 106(1): 011101
5. Sheu J K, Chi G C, Jou M J. Low-operation voltage of InGaN/GaN light-emitting diodes by using a Mg-doped $Al_{0.15}Ga_{0.85}N$/GaN superlattice. IEEE Electron Device Letters, 2001, 22(4): 160–162
6. Jang J S, Kim D, Seong T Y. Low turn-on voltage and series resistance of polarization-induced InGaN-GaN LEDs by using *p*-InGaN/*p*-GaN superlattice. IEEE Photonics Technology Letters, 2006, 18(4): 1536–1538
7. Jang J S, Sohn S J, Kim D, Seong T Y. Formation of low-resistance transparent Ni/Au ohmic contacts to a polarization field-induced *p*-InGaN/GaN superlattice. Semiconductor Science and Technology, 2006, 21(5): L37–L39
8. Liu Y J, Tsai T Y, Yen C H, Chen L Y, Tsai T H, Liu W C. Characteristics of a GaN-based light-emitting diode with an inserted *p*-GaN/*i*-InGaN superlattice structure. IEEE Journal of Quantum Electronics, 2010, 46(4): 492–498
9. Liu Y J, Guo D F, Chu K Y, Cheng S Y, Liou J K, Chen L Y, Tsai T H, Huang C C, Chen T Y, Hsu C S, Tsai T Y, Liu W C. Improved current-spreading performance of an InGaN-based light-emitting diode with a clear *p*-GaN/*n*-GaN barrier junction. Displays, 2011, 32 (5): 330–333
10. Jang J S. High output power GaN-based light-emitting diodes using an electrically reverse-connected *p*-Schottky diode and *p*-InGaN–GaN superlattice. Applied Physics Letters, 2008, 93(8): 081118
11. Hsu C Y, Lan W H, Wu W S. Effect of thermal annealing of Ni/Au ohmic contact on the leakage current of GaN based light emitting diodes. Applied Physics Letters, 2003, 83(12): 2447
12. Li D S, Chen H, Yu H B, Jia H Q, Huang Q, Zhou J M. Dependence of leakage current on dislocations in GaN-based light-emitting diodes. Journal of Applied Physics, 2004, 96(2): 1111
13. Lin Y J. Application of the thermionic field emission model in the study of a Schottky barrier of Ni on *p*-GaN from current-voltage measurements. Applied Physics Letters, 2005, 86(12): 122109
14. Pan Y B, Yang Z J, Lu Y, Lu M, Hu C Y, Yu T J, Hu X D, Zhang C Y. Improvement of properties of *p*-GaN by Mg delta doping. Chinese Physics Letters, 2004, 21(10): 2016
15. Wang H, Liu J, Niu N, Shen G, Zhang S. Enhanced performance of *p*-GaN by Mg doping. Journal of Crystal Growth, 2007, 304(1): 7–10
16. Bayram C, Pau J L, McClintock R, Razeghi M. Delta-doping optimization for high quality *p*-type GaN. Journal of Applied Physics, 2008, 104(8): 083512
17. Park H Y, Jeon K N, Kim K. Mg delta-doping effect on a deep hole center related to electrical activation of a *p*-type GaN thin film. Transactions on Electrical and Electronic Materials, 2010, 11(1): 37–41
18. Marlow G S, Das M B. The effects of contact size and non-zero metal resistance on the determination of specific contact resistance. Solid-State Electronics, 1982, 25(2): 91–94
19. Jang J S, Seong T Y, Jeon S R. Formation mechanisms of low-resistance and thermally stable Pd/Ni/Pd/Ru Ohmic contacts to Mg-doped $Al_{0.15}Ga_{0.85}N$. Applied Physics Letters, 2007, 91(9): 092129
20. Jang J S, Seong T Y. Electronic transport mechanisms of nonalloyed Pt Ohmic contacts to *p*-GaN. Applied Physics Letters, 2000, 76(19): 2743
21. Jang S H, Jang J S. Carrier transport mechanism at the interface between metals and p-type III-nitrides having different surface electronic structure. Japanese Journal of Applied Physics (in press)
22. Jang J S, Chang I S, Kim H K, Seong T Y, Lee S H, Park S J. Low-resistance Pt/Ni/Au ohmic contacts to *p*-type GaN. Applied Physics Letters, 1999, 74(1): 70